Validating surface downwelling solar irradiances estimated by the McClear model under cloud-free skies in the United Arab Emirates

Yehia Eissa, Saima Munawwar, Armel Oumbe, Philippe Blanc, Hosni Ghedira, Lucien Wald, Hélène Bru, Dominique Goffe

Available online at www.sciencedirect.com

ScienceDirect

Solar Energy 114 (2015) 17–31

SOLAR ENERGY

www.elsevier.com/locate/solener

Validating surface downwelling solar irradiances estimated by the McClear model under cloud-free skies in the United Arab Emirates

Yehia Eissa [a,b,*], Saima Munawwar [b], Armel Oumbe [c], Philippe Blanc [a], Hosni Ghedira [b], Lucien Wald [a], Hélène Bru [c], Dominique Goffe [d]

[a] MINES ParisTech, PSL Research University, O.I.E. – Centre Observation, Impacts, Energy, CS 10207 – 06904 Sophia Antipolis cedex, France
[b] Masdar Institute, Research Center for Renewable Energy Mapping and Assessment, Abu Dhabi, PO Box 54224, United Arab Emirates
[c] Total New Energies, R&D Solar, 92069 Paris La Défense, France
[d] Bertin Technologies, Energy Process Environment Department, 40220 Tarnos, France

Received 1 April 2014; received in revised form 18 December 2014; accepted 15 January 2015

Communicated by: Associate Editor David Renne

Abstract

McClear, a fast model based on a radiative transfer solver, exploits the atmospheric properties provided by the EU-funded MACC project (Monitoring Atmospheric Composition and Climate) to estimate the surface downwelling solar irradiances for cloud-free instances. This article presents the first validation of the McClear model for the specific climate of the United Arab Emirates where skies are frequently cloud-free but turbid. McClear accurately estimates the global horizontal irradiance measured every 10 min at seven sites. The bias ranges from -9 W m^{-2} (-1% of the mean observed irradiance) to $+35$ W m^{-2} ($+6$%). The root mean square error (RMSE) ranges from 22 W m^{-2} (4%) to 47 W m^{-2} (8%) and the coefficient of determination ranges from 0.980 to 0.990. Estimates of the direct irradiance at normal incidence exhibit an underestimation that is attributed to the overestimation of the aerosol optical depth in the MACC data set and not accounting for the circumsolar radiation in McClear. The corresponding bias ranges from -57 W m^{-2} (-8%) to $+6$ W m^{-2} ($+1$%). The RMSE ranges from 62 W m^{-2} (9%) to 87 W m^{-2} (13%) and the coefficient of determination ranges from 0.830 to 0.863. When compared to two other models in the literature, McClear is better able to capture the temporal variability of the direct irradiance at normal incidence. The validation results remain comparable for the global horizontal irradiance.

Keywords: Aerosols; Atmosphere; MACC; Solar radiation

1. Introduction

Accurate assessments of the solar resource are valuable for numerous applications, e.g. weather, climate, biomass, and of course solar energy. Due to the limited number of ground solar radiation measurement stations and the inaccuracy of interpolation methods between stations many models use satellite observations to estimate the solar radiation at ground level in a dense manner in space and in

* Corresponding author at: MINES ParisTech, Centre Observation, Impacts, Energy, CS 10207 – 06904 Sophia Antipolis cedex, France. Tel.: +33 (0)4 93 95 74 65; fax: +33 (0)4 93 67 89 08.

E-mail addresses: yehia.eissa@mines-paristech.fr (Y. Eissa), smunawwar@masdar.ac.ae (S. Munawwar), armel.oumbe@total.com (A. Oumbe), philippe.blanc@mines-paristech.fr (P. Blanc), hghedira@masdar.ac.ae (H. Ghedira), lucien.wald@mines-paristech.fr (L. Wald), helene.bru@total.com (H. Bru), goffe@bertin.fr (D. Goffe).

http://dx.doi.org/10.1016/j.solener.2015.01.017
0038-092X/

Acronyms

AERONET Aerosol Robotic Network
a.m.s.l. altitude above mean sea level
AOD aerosol optical depth
AOD_{550} aerosol optical depth at 550 nm
BSRN Baseline Surface Radiation Network
CC correlation coefficient
DHI diffuse horizontal irradiance
DNI direct normal irradiance, i.e. direct irradiance at normal incidence
E-ANN ensemble artificial neural network
ESRA European Solar Radiation Atlas
GHI global horizontal irradiance
HC3v4 HelioClim-3v4
LS least-squares
MACC Monitoring Atmospheric Composition and Climate
MATCH Model of Atmospheric Transport and Chemistry
MODIS Moderate Resolution Imaging Spectroradiometer
mref mean of observed (reference) values
ndata number of samples
PREDISOL Predicting Solar Radiation
R^2 coefficient of determination
RMSE root mean square error
RSI rotating shadowband irradiometer
SSI surface solar irradiance
UAE United Arab Emirates
WMO World Meteorological Organization

Symbols

B downwelling direct (or beam) solar irradiance received on a horizontal surface (W m^{-2})
B_n downwelling direct (or beam) solar irradiance received on a surface normal to the Sun rays (W m^{-2})
E_0 top of atmosphere irradiance received on a horizontal surface (W m^{-2})
E_{0n} top of atmosphere irradiance received on a surface normal to the Sun rays (W m^{-2})
G downwelling global solar irradiance received on a horizontal surface (W m^{-2})
KT clearness index (unitless)
KT_B direct clearness index (unitless)
KT_{Bn} direct normal clearness index (unitless)
α Ångström coefficient (unitless)
β aerosol optical depth at 1000 nm (unitless)
θ_S solar zenith angle (deg)
λ wavelength (nm)
τ_λ aerosol optical depth at wavelength λ (unitless)

time at a large temporal and spatial coverage (see e.g. Cano et al., 1986; Perez et al., 2002; Rigollier et al., 2004; Schillings et al., 2004; Sun and Liu, 2013; Qu et al., 2012a, 2012b; Zelenka et al., 1999). The solar radiation at ground level is also known as the surface solar irradiance (SSI), the surface solar radiation or the surface downwelling solar radiation. In cloud-free conditions, variable atmospheric parameters, namely aerosols and water vapour, are key factors in estimating the SSI and their accurate knowledge is required for accurate estimations (Lefevre et al., 2013; Oumbe et al., 2012a, 2013; Schroedter-Homscheidt and Oumbe, 2013).

A model that accurately estimates the SSI under cloud-free skies is of particular importance in determining the upper limit of the irradiance for a given location and instant. Furthermore, Oumbe et al. (2014) showed that in the case of infinite plane-parallel single- and double-layered cloud, the SSI computed by a radiative transfer model can be approximated with a great accuracy by the product of the SSI under cloud-free skies and a modification factor due to cloud properties and ground albedo only. Changes in clear-atmosphere properties have negligible effect on the latter so that both terms can be calculated independently.

McClear (Lefevre et al., 2013) is a physical model based on look-up-tables established with the radiative transfer model libRadtran (Mayer and Kylling, 2005; Mayer et al., 2012) with the aim to accurately predict the downwelling broadband global horizontal irradiance (GHI), direct –or beam– horizontal irradiance, direct irradiance at normal incidence, abbreviated in direct normal irradiance (DNI), and diffuse horizontal irradiance (DHI) at ground level for cloud-free skies. Other cloud-free solar irradiance prediction models are available in the literature (Gueymard, 2012; Ineichen, 2006). An interesting feature of McClear is its design based on look-up-tables permits a very fast execution: it runs 100,000 times faster than libRadtran. Another feature is that McClear can be run as a Web service, using as inputs the reanalysis data set of atmospheric composition available worldwide from 2004 provided by the MACC project (Monitoring Atmospheric Composition and Climate) –funded by the European Commission– (Benedetti et al., 2009; Inness et al., 2013; Schroedter-Homscheidt et al., 2013).

The ten input parameters to McClear are: the solar zenith angle (Blanc and Wald, 2012), the ground albedo, the altitude of the ground level, the elevation above ground, the aerosol optical depth at 550 nm (AOD_{550}), the Ångström coefficient (Ångström, 1964), the aerosol type (Hess et al., 1998), the total column contents in ozone and water vapour and the atmospheric profile, i.e. the vertical profiles of temperature, pressure, density and volume

mixing ratio for gases (Anderson et al., 1986). The aerosol types and atmospheric profiles used in McClear are the same ones included in libRadtran. McClear also makes use of a worldwide set of 12 monthly maps of ground albedo parameters (Blanc et al., 2014b) that are derived from the MODIS (Moderate Resolution Imaging Spectroradiometer) products MCD43C1 and MCD43C2 (Schaaf et al., 2002).

The McClear model with inputs from MACC and MODIS is available as a Web service, i.e. an application that can be invoked *via* the Web. An interface has been developed to launch McClear within a standard Web browser *via* the catalogue of products on the MACC Web site (http://www.gmes-atmosphere.eu). Users need only to specify the latitude, longitude, the altitude of the site (optionally), time period of interest and the integration period of the solar radiation: 1 min, 15 min, 1 h, 1 day.

McClear has been previously validated (Lefevre et al., 2013) with respect to 1 min GHI and direct horizontal irradiance measurements from the Baseline Surface Radiation Network (BSRN) collected from 11 sites located throughout six continents. The BSRN network is described in Ohmura et al. (1998). The bias relative to the mean of the measurements, ranges from −1% to +4% (GHI) and −7 to +1% (direct horizontal irradiance), while the relative root mean square error (RMSE) ranges from 3% to 5% (GHI) and 5% to 11% (direct horizontal irradiance).

The United Arab Emirates (UAE) is a region which has ambitious plans for energy production from solar powered plants (Eissa et al., 2012; Mezher et al., 2011; Mokri et al., 2013). The climate of the UAE is specific as the cloud coverage is low, and the cloud-free skies range from being highly turbid due to high dust concentrations to "Rayleigh-like" blue skies (Gherboudj and Ghedira, 2014). The validation performed by Lefevre et al. (2013) does not include such specific conditions. The present work palliates this shortcoming and compares McClear estimates of the GHI and the DNI against measurements made every 10 min at seven stations in the UAE. The paper is organized as: description of the ground measurements (Section 2), validation results (Section 3), discussion on the MACC estimated aerosols and a comparison with two other irradiance estimation models (Section 4) and finally the conclusions (Section 5).

2. UAE ground measurements for validation

2.1. Solar irradiance ground measurements

The emirate of Abu Dhabi covers 87% of the land area of the UAE. It includes the variety of landscapes found in the UAE. A network of six stations has been installed in the emirate by Masdar Clean Energy. The company CSP Services installed the stations, performed their calibrations and provided the measurements at a 10 min temporal step (Geuder et al., 2014). The six stations are scattered throughout the emirate (Fig. 1 and Table 1) and are deemed to represent the climate of the UAE. Masdar City is located in the suburbs of Abu Dhabi (the city and capital), where the environment is near-coastal, desert and urban. The surrounding environment of the Madinat Zayed station is desert and it is located at Shams 1, a 100 MW concentrating solar thermal electric plant (Al Jaber, 2013). The surrounding environments of the three stations: Al Sweihan, Al Aradh and Al Wagan are similar to that of Madinat Zayed. The station East of Jebel Hafeet is situated near a rocky mountainous area and its altitude is slightly greater than the other five stations.

For all six stations, the irradiances were measured using a Rotating Shadowband Irradiometer (RSI). The RSI is a silicon photodiode, the LI-COR LI-200 Pyranometer, integrated with a rotating shadowband. This pyranometer has a spectral range from 400 nm to 1100 nm, and was calibrated against an Eppley Precision Spectral Pyranometer under natural daylight conditions (http://www.licor.com/env/products/light/pyranometers). CSP Services performed another calibration of the RSI measured irradiances with respect to a high precision meteorological station at Plataforma Solar de Almeria and it has checked that such a calibration is suitable for other sites in the Middle East and North Africa region (Geuder et al., 2014). During acquisition, the GHI is measured when the shadowband is stationary below the horizon of the photodiode and the DHI is measured when the rotating shadowband masks the entire solar disc from the pyranometer. The shadowband rotates once per minute. The direct horizontal irradiance is then computed by subtracting the DHI from the GHI. The DNI is computed from the direct horizontal irradiance and the solar zenith angle. In our case, the irradiances were averaged over 10 min. Only those measurements for the full year 2012 which passed the quality check procedures of Roesch et al. (2011) were used for validation.

A seventh meteorological station is used and is also located in Madinat Zayed 500 m apart that of Masdar. It was installed by the company Bertin Technologies in the framework of the PREDISOL (PREDIcting SOLar radiation) project (Oumbe et al., 2012a, 2013). The GHI and DHI were measured respectively by one unshaded and one shaded Kipp and Zonen CMP11 pyranometers (http://www.kippzonen.com) that comprise a thermopile covering the spectral range from 285 nm to 2800 nm. The DNI was measured by the Kipp and Zonen CHP1 pyrheliometer that comprises a thermopile covering the spectral range from 200 nm to 4000 nm. The sampling rate of the instruments was 1 s. Measurements were averaged over 1 min.

To match the temporal step of 10 min of the six Masdar stations, measurements from the Bertin station and the McClear estimates were averaged over 10 min provided all 1 min measurements within the period were present – i.e. no missing values– and valid according to the quality check procedures of Roesch et al. (2011). Then the algorithm of Long and Ackerman (2000) was applied to these 10 min data sets in order to retain reliable cloud-free

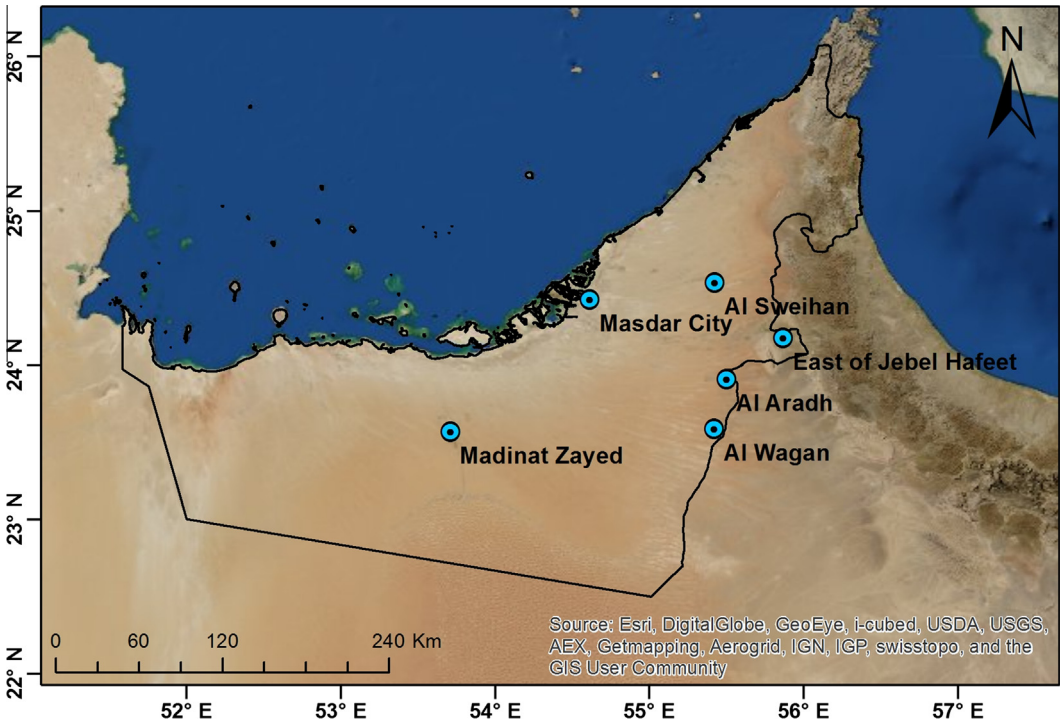

Fig. 1. Locations of the six stations in the UAE.

Table 1
Coordinates, abbreviations and altitudes above mean sea level (a.m.s.l.) of the stations equipped with a RSI.

Location	Station Code	Latitude (°N)	Longitude (°E)	a.m.s.l. (m)
Al Aradh	AR	23.903	55.499	178
East of Jebel Hafeet	EJH	24.168	55.864	341
Masdar City	MasdC	24.420	54.613	7
Madinat Zayed	MZ	23.561	53.709	137
Al Sweihan	SW	24.530	55.423	175
Al Wagan	WA	23.579	55.419	142

instants. The first and third tests of Long and Ackerman, namely the normalized total shortwave magnitude test and the change in magnitude with time test, were kept unchanged. In the second test, the maximum diffuse shortwave test, the maximum DHI was empirically set at 300 W m^{-2}, instead of the 150 W m^{-2} suggested by Long and Ackerman, to better represent the local conditions of the UAE. The fourth and final test, the normalized diffuse ratio variability test, was modified to accommodate for the 10 min time step instead of the 1 min time step of Long and Ackerman. The time span was changed from 11 min to 30 min and the threshold on the standard deviation of the normalized diffuse fraction was empirically set at 0.02. As an average, 37% of valid data were retained as cloud-free.

If G denotes the GHI, B the direct horizontal irradiance, B_n the DNI, E_0 the horizontal irradiance at the top of the atmosphere and E_{0n} is the normal irradiance at the top of the atmosphere, the clearness index KT, also called the global transmissivity of the atmosphere, is computed as:

$$KT = G/E_0. \quad (1)$$

Similarly the direct clearness index (KT_B) is defined as:

$$KT_B = B/E_0. \quad (2)$$

The direct normal clearness index KT_{Bn} is also defined, but with respect to E_{0n}:

$$KT_{B_n} = B_n/E_{0n}. \quad (3)$$

One notes that $KT_B = KT_{Bn}$ because $B = B_n\cos(\theta_S)$ where θ_S denotes the solar zenith angle.

2.2. AERONET ground measurement campaigns

Ground measurements from the NASA AERONET (AErosol RObotic NETwork) program are available over the UAE from 16 stations (Holben et al., 1998). The majority of the measurements were collected during the UAE Unified Aerosol Experiment which commenced in the year 2004, providing a remarkably increased AERONET data availability in the Middle East (Reid et al., 2005). The measurements at several AERONET stations correspond to short measurement campaigns for limited periods of time. Only five stations in the UAE have more than one year of measurements.

For each AERONET station, the measurements of the CIMEL CE-318 Sun photometer were converted into aerosol optical properties and are available for public access (http://aeronet.gsfc.nasa.gov). The data sets include the aerosol optical depth (AOD) at eight different wavelengths, as well as the solar zenith angle and the total column content in water vapour. The AERONET Level 2.0 products

(cloud-screened and quality assured) are compared in Section 4.1 to the AOD_{550} from MACC for a better understanding of the errors found in the McClear estimates.

3. Validation of McClear in the UAE

In this section the validation results of the McClear estimates for the GHI, DNI, clearness index and direct normal clearness index are presented for cloud-free instances. The deviations were computed by subtracting measurements for each instant from the McClear estimates. Three statistical measures were computed: bias, RMSE and the coefficient of determination (R^2). Therefore, a positive bias corresponds to an overestimation by McClear and *vice versa*. Relative values are expressed with respect to the mean observed value. Only four scatter density plots displaying the McClear values versus the ground measured –or derived– values are presented for two of the seven meteorological stations. The selected stations are AR (desert surrounding) and MasdC (near-coastal location exposed to desert, marine and anthropogenic aerosols). The figures also present the number of samples (ndata), the mean of observed values (mref), the bias, the RMSE, the correlation coefficient (CC), the 1:1 line ($x = y$) and the least-squares (LS) affine regression ($x = ay + b$). The validation results from all seven stations are presented in Tables 2–5.

The scatter density plot of the GHI estimated from McClear versus that measured at AR station is shown in Fig. 2. It is apparent that there is a high agreement between the McClear GHI and the measured GHI. Most observations lie around the 1:1 line and the scatter around this line is low. The relative bias is −1%, the relative RMSE is 5% and R^2 is 0.986. Comparing the relative bias and RMSE with those reported by Gueymard (2012) who compared 18 broadband radiative models over Solar Village in Saudi Arabia, the errors of the McClear estimates are less than those of simple radiation models and comparable to those of the most detailed models. It can be concluded that McClear provides accurate results of the GHI over the site AR. The slight underestimation may be due to an overestimation in the AOD_{550} extracted from the MACC reanalysis data set, which will be discussed in Section 4.1.

The scatter density plot of the DNI estimated from McClear versus the ground-derived DNI is shown in Fig. 3. In this case there is an underestimation for most of the observations, both low and high values. The scatter around the best fit line is more noticeable than for the GHI. All statistical measures exhibit poorer performances than those for the GHI. The relative bias is −8%, the relative RMSE is 13% and R^2 is 0.846. The bias is attributed to two causes. The first is an overestimation in the AOD_{550} input to McClear. Aerosols directly affect the DNI but their effect is less pronounced on the GHI, which may explain the difference in the scatter observed in the two plots. The second cause is the circumsolar radiation, which is the radiation which encounters forward scattering in the very near vicinity of the solar disc as a result of the large particles present in the atmosphere, i.e. dust and thin cirrus

Table 2
Validations of cloud-free global horizontal irradiances estimated by McClear. Overall is for all measurements from all stations combined.

Station	# of samples	Mean	Bias		RMSE		R^2
		W m^{-2}	W m^{-2}	%	W m^{-2}	%	
AR	7955	637.9	−9	−1	29	5	0.986
EJH	9090	609.0	+9	+1	25	4	0.988
MasdC	7241	557.6	+35	+6	47	8	0.980
MZ_{masd}	4755	582.1	+18	+3	29	5	0.990
MZ_{bertin}	4755	603.3	−5	−1	22	4	0.990
SW	8230	585.1	+18	+3	31	5	0.988
WA	9320	618.3	−1	0	25	4	0.988
Overall	51346	601.1	+9	+2	31	5	0.982

Table 3
Validations of cloud-free direct normal irradiances estimated by McClear. Overall is for all measurements from all stations combined.

Station	# of samples	Mean	Bias		RMSE		R^2
		W m^{-2}	W m^{-2}	%	W m^{-2}	%	
AR	7955	689.9	−57	−8	87	13	0.846
EJH	9090	682.8	−15	−2	62	9	0.850
MasdC	7241	634.2	+6	+1	62	10	0.830
MZ_{masd}	4755	670.3	−25	−4	64	10	0.863
MZ_{bertin}	4755	680.9	−42	−6	74	11	0.857
SW	8230	660.1	−16	−2	63	10	0.850
WA	9320	668.4	−41	−6	74	11	0.861
Overall	51346	669.5	−27	−4	70	11	0.837

Table 4
Validations of cloud-free clearness index estimated by McClear. Overall is for all measurements from all stations combined.

Station	# of samples	Mean	Bias		RMSE		R^2
		Unitless	Unitless	%	Unitless	%	
AR	7955	0.71	−0.01	−1	0.03	5	0.817
EJH	9090	0.69	+0.01	+2	0.03	5	0.830
MasdC	7241	0.65	+0.04	+7	0.06	9	0.731
MZ_{masd}	4755	0.68	+0.02	+3	0.03	5	0.856
MZ_{bertin}	4755	0.70	−0.01	−1	0.03	4	0.848
SW	8230	0.68	+0.02	+3	0.04	6	0.824
WA	9320	0.70	0	0	0.03	4	0.850
Overall	51346	0.69	+0.01	+2	0.04	6	0.773

Table 5
Validations of cloud-free direct normal clearness index estimated by McClear. Overall is for all measurements from all stations combined.

Station	# of samples	Mean	Bias		RMSE		R^2
		Unitless	Unitless	%	Unitless	%	
AR	7955	0.50	−0.04	−8	0.06	13	0.839
EJH	9090	0.49	−0.01	−2	0.05	9	0.843
MasdC	7241	0.46	0	+1	0.05	10	0.824
MZ_{masd}	4755	0.48	−0.02	−4	0.05	10	0.859
MZ_{bertin}	4755	0.49	−0.03	−6	0.05	11	0.854
SW	8230	0.48	−0.01	−3	0.05	10	0.843
WA	9320	0.48	−0.03	−6	0.05	11	0.852
Overall	51346	0.48	−0.02	−4	0.05	11	0.830

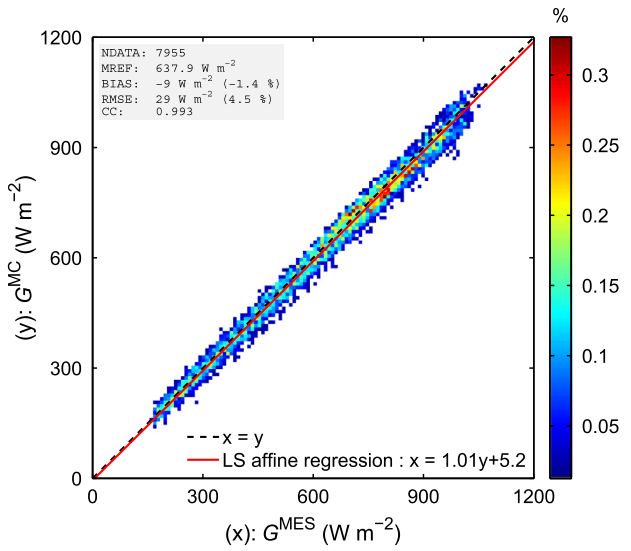

Fig. 2. Scatter density plot of McClear (G^{MC}) versus RSI (G^{MES}) global horizontal irradiance over Al Aradh, 2012.

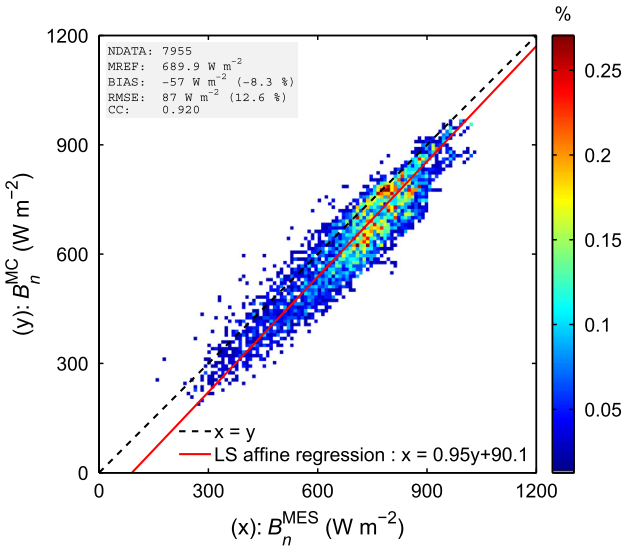

Fig. 3. Scatter density plot of McClear (B_n^{MC}) versus RSI (B_n^{MES}) direct normal irradiance over Al Aradh, 2012.

clouds (Blanc et al., 2014a; Buie et al., 2003; Eissa et al., 2014; Oumbe et al., 2012b; Wilbert et al., 2013). Even though the circumsolar radiation is diffuse radiation, it is still intercepted within the field of view of the recommended measurement systems (WMO, 2010) for which the aperture half-angle is 2.5° with a non-null sensitivity for up to 4°. The current version of McClear does not account for the circumsolar radiation, despite it is being measured by the ground instrumentation. This contributes to the observed underestimation.

Fig. 4 exhibits the scatter density plot of the clearness indices estimated from McClear versus these derived from measurements at the station AR. The relative bias is −1% and the relative RMSE is 5%, and are very similar to those obtained by the McClear GHI. However, R^2 is less than for GHI: 0.817 versus 0.986. The changes in solar radiation at the top of the atmosphere due to changes in geometry, namely the daily course of the Sun and seasonal effects, are usually well reproduced by models and lead to a *de facto* correlation between observations and estimates of the GHI (or DNI) hiding potential weaknesses. The clearness indices are stricter indicators of the performances of a model regarding its ability to estimate the optical state of the atmosphere. Though the clearness indices are not completely independent of the solar zenith angle as they decrease as the solar zenith angle increases, the dependency is much less pronounced than in the GHI or DNI. This explains why the correlation coefficient is less for the clearness index than for the GHI. Nonetheless, the observations are well scattered along the 1:1 line.

The direct normal clearness indices estimated from McClear are plotted against these derived from measurements in Fig. 5. The statistical indicators exhibit similar values to those of the DNI validation and the scatter along the line of best fit is limited.

When assessing the performance of McClear at the MasdC site, it is apparent that the McClear GHI is overestimated. The scatter density plot is shown in Fig. 6, and the relative bias is +6%, the relative RMSE is 8% and R^2 is 0.980. Even though the relative RMSE is satisfactory, there is an almost constant overestimation of the McClear GHI for most of the GHI range. This bias can be attributed to the overestimation of the DHI by McClear as there is negligible bias in the McClear DNI over this station. The validation indicators for the McClear DNI over MasdC (*cf.* Fig. 7) exhibit a relative bias of +1%, a relative RMSE of 10% and R^2 is 0.830. The scatter around the line of best fit is greater than that for the GHI.

The validations of the McClear clearness index (*cf.* Fig. 8) and the McClear direct normal clearness index (*cf.* Fig. 9) over MasdC are similar to those of AR. The rel-

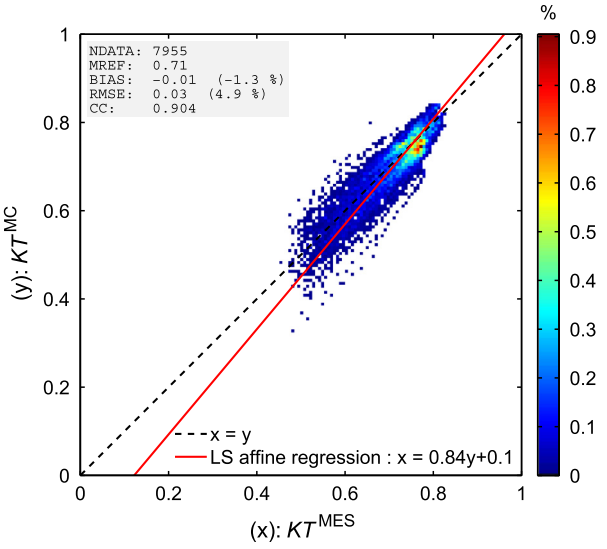

Fig. 4. Scatter density plot of McClear (KT^{MC}) versus RSI (KT^{MES}) clearness index over Al Aradh, 2012.

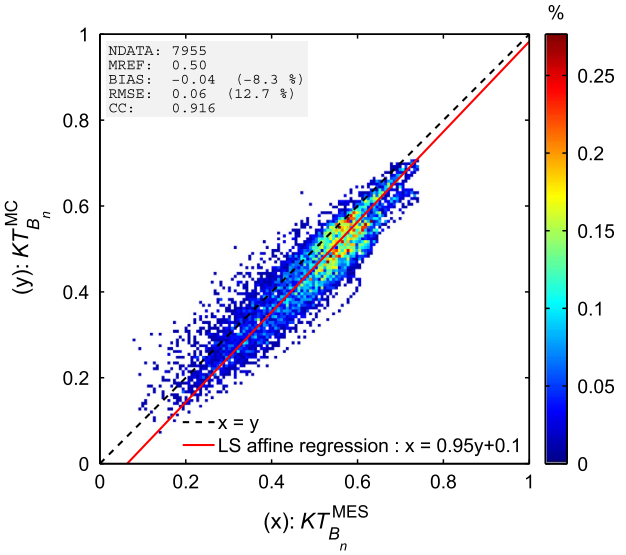

Fig. 5. Scatter density plot of McClear ($KT_{Bn}{}^{MC}$) versus RSI ($KT_{Bn}{}^{MES}$) direct normal clearness index over Al Aradh, 2012.

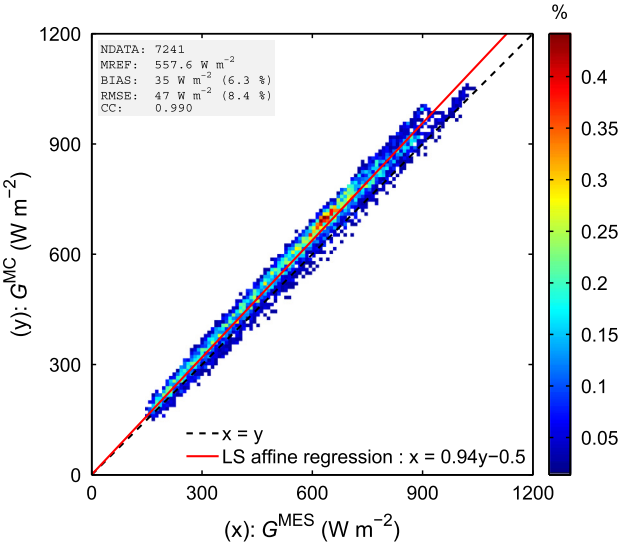

Fig. 6. Scatter density plot of McClear (G^{MC}) versus RSI (G^{MES}) global horizontal irradiance over Masdar City, 2012.

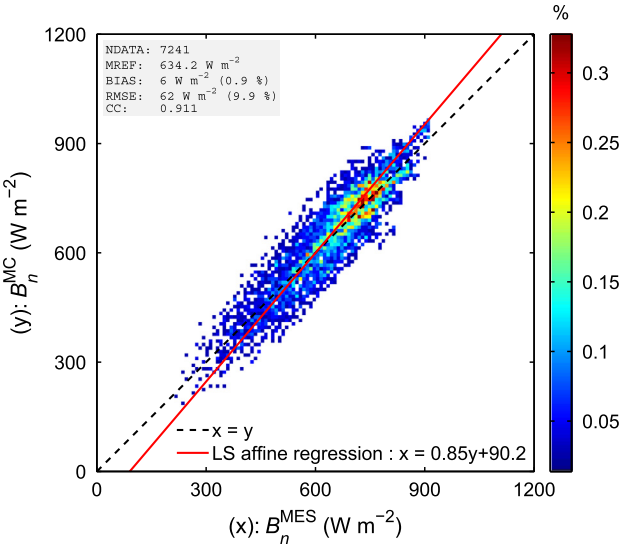

Fig. 7. Scatter density plot of McClear ($B_n{}^{MC}$) versus RSI ($B_n{}^{MES}$) direct normal irradiance over Masdar City, 2012.

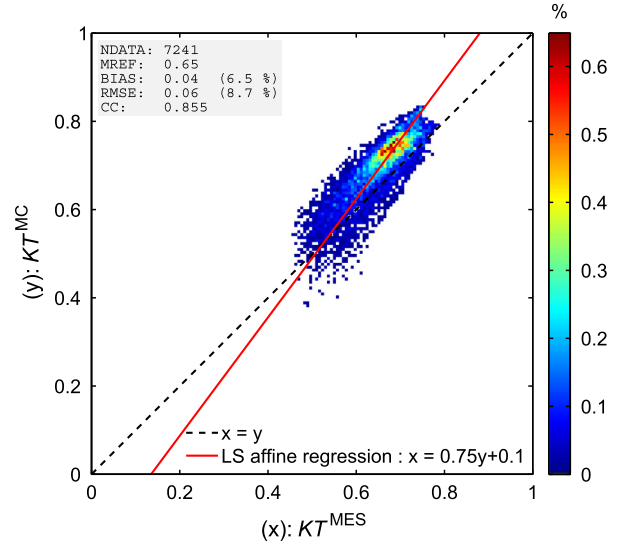

Fig. 8. Scatter density plot of McClear (KT^{MC}) versus RSI (KT^{MES}) clearness index over Masdar City, 2012.

ative bias and relative RMSE remain close to those obtained by the McClear GHI and the McClear DNI, respectively. A noticeably lower R^2 value is present for the McClear clearness index when compared to that of the McClear GHI.

Tables 2–5 respectively present the statistical indicators for the deviations between the estimated and ground measured –or derived– GHI, DNI, clearness index and direct normal clearness index for all seven validation stations. The statistical indicators are coherent between the stations, and no single station stands out. The differences between the Masdar MZ station (MZ_{masd}) and the Bertin MZ station (MZ_{bertin}) are due to the different instruments. When comparing the measured GHI and DNI at both stations for the same cloud-free instants, differences of 4% in relative RMSE and −4% in relative bias for GHI, and 3% in relative RMSE and −2% in relative bias for DNI, were observed. In this case the RSI irradiances were underestimated with respect to those measured by the Kipp and Zonen pyranometer and pyrheliometer. The measurements from the Kipp and Zonen instruments at the Bertin MZ station were taken as the reference values because (1) they correspond to the standard measurements recommended by the WMO (2010) and (2) the radiometers were cleaned on a daily basis. These errors explain the differences in the validations between both stations.

For the McClear GHI the relative bias ranges from −1% to +6%, relative RMSE ranges from 4% to 8% and R^2 ranges from 0.980 to 0.990. Generally the McClear esti-

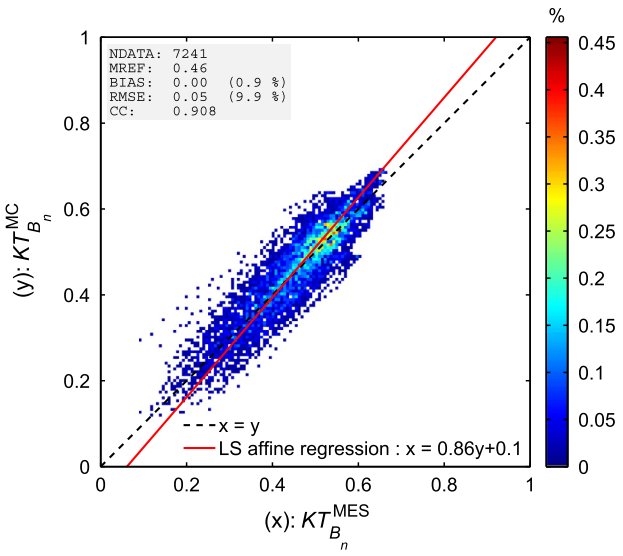

Fig. 9. Scatter density plot of McClear (KT_{Bn}^{MC}) versus RSI (KT_{Bn}^{MES}) direct normal clearness index over Masdar City, 2012.

mates are satisfactory, with low relative RMSE values. The bias is also low, but it can be further improved with inputs of better quality, *cf.* Section 4.1. When comparing the results in Table 2 to those previously obtained by McClear over 11 different stations around the globe (Lefevre et al., 2013), it is found that the relative bias is within the reported range of −1% to +4%, and the relative RMSE is also within the reported range of 3% to 5% for all stations, except for MasdC which exhibits a relative bias of +6% and a relative RMSE of 8%. This could be explained by the mixed nature of this site, which can be described as a near-coastal station exposed to desert, marine and anthropogenic aerosols.

The McClear DNI estimates exhibit slightly poorer performances when compared to those of McClear GHI, but they still remain satisfactory. The relative bias in Table 3 ranges from −8% to +1%, the relative RMSE ranges from 9% to 13% and R^2 ranges from 0.830 to 0.863. There is an underestimation in the McClear DNI for all stations but MasdC. An overestimation in the MACC AOD_{550} across the region of the UAE causes an underestimation in the McClear DNI. Accounting for the circumsolar irradiance in McClear would lead to improved results.

The three stations exhibiting the greatest relative bias in the DNI estimates are AR (−8%), MZ_{bertin} (−6%) and WA (−6%). These three stations have similar surroundings and this may imply that the MACC AOD_{550} is more overestimated in some regions than in others. The stations SW and EJH can probably be grouped together, as they are ∼60 km apart and they have the same relative bias of −2%. Due to the limited number of stations no strong conclusion in spatial distribution of the estimation error can be drawn and it could be fortuitous for the studied period. The 1.125° spatial resolution of MACC could not possibly depict the local atmospheric characteristics of a point location.

Tables 4 and 5 present the statistical indicators for the McClear clearness index and direct normal clearness index. The relative bias and relative RMSE are close to those obtained for the McClear GHI and DNI, respectively. The R^2 values are always less for the McClear clearness index than for the McClear GHI for the same stations.

Taking into account the accuracy of the RSI instrument, ±4.7% (GHI) and ±4.1% (DNI) as reported by CSP Services with the measurements themselves, it is reasonable to state that McClear provides satisfactory GHI and DNI estimates for cloud-free observations over the environment of the UAE.

4. Discussion

This section presents a comparison between the AOD_{550} from AERONET level 2.0 products and from MACC for a better understanding on the errors observed in the McClear irradiances. It is followed by a comparison between McClear and two other irradiance estimation models under cloud-free conditions.

4.1. AERONET versus MACC aerosol optical depths

The AERONET data sets do not provide the AOD_{550} directly, as measurements are not collected at the exact wavelength of 550 nm. For the sake of comparison with MACC AOD_{550}, the AERONET AOD_{550} is computed by the Ångström law:

$$\tau_\lambda = \beta(\lambda)^{-\alpha}, \tag{4}$$

$$\ln(\tau_\lambda) = \ln(\beta) - \alpha\ln(\lambda), \tag{5}$$

where τ_λ is the AOD at wavelength λ, λ is the wavelength presented in μm, β is the AOD at 1000 nm and α is the Ångström coefficient. The α and β coefficients were computed by linearly transforming Eq. (4) into Eq. (5) and fitting $\ln(\tau_\lambda)$ with $\ln(\lambda)$ from the AODs available from AERONET for the wavelength interval [440 nm, 870 nm], where the slope of this linear fit is $-\alpha$ and the intercept is $\ln(\beta)$. The time sampling of the AERONET Level 2.0 product is irregular and varies from a few seconds to hours, while MACC has a temporal resolution of 3 h. Therefore, the MACC observations were interpolated in space and in time to match the AERONET acquisition time and the location of the site in question.

The AOD_{550} from MACC are compared to those from AERONET at each of the 16 AERONET stations in the UAE. Fig. 10 exhibits the locations of the stations. It displays the differences between the MACC and AERONET AOD_{550} expressed as the RMSE shown in different colors. The size of the disc over each station is proportional to the mean AOD_{550} at that location. The mean AOD_{550} ranges from 0.3 to 1.0, and is 0.4 at most locations. The RMSE ranges from 0.08 to 0.28 and is between 0.12 and 0.20 for most stations. The relative RMSE ranges between 20% and 100%. MACC overestimates the AOD_{550} at each sta-

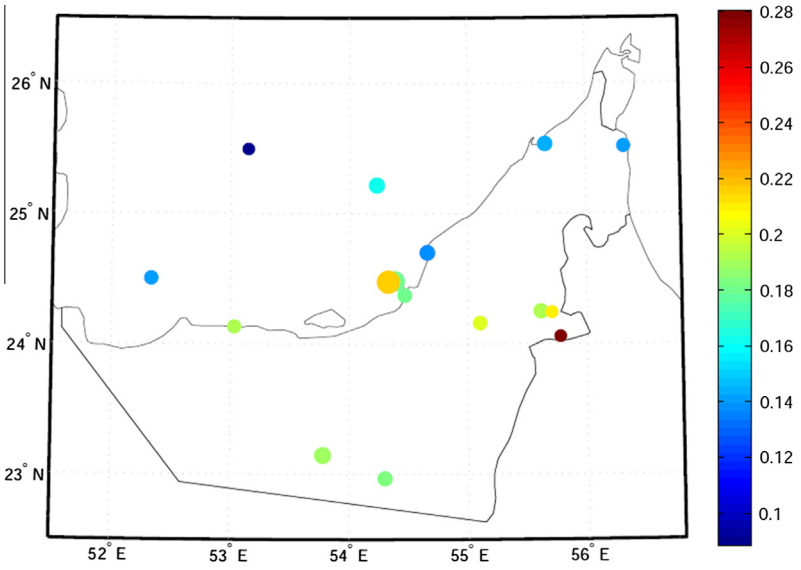

Fig. 10. RMSE between MACC AOD_{550} and AERONET AOD_{550} for each of the stations, shown in different colors. The size of the disc over each station is proportional to the mean AOD_{550} at that specific location.

tion; the bias ranges from 0.05 to 0.25. The relative bias is low for most stations: between 10% and 20% for 10 of the 16 stations, but it can be very high (i.e. 80% at one station). The correlation coefficient is relatively high at all stations. It is greater than 0.7 for 14 of the 16 stations, which shows that MACC reproduces satisfactorily the temporal variability of the AOD_{550}.

The above findings add evidence to the already reported overestimation of the MACC AOD_{550} with respect the AERONET observations over the region of the UAE (Benedictow et al., 2014; Oumbe et al., 2013). The positive bias at latitudes close to that of the UAE is attributed to major dust sources, sulfate and organic matter. This is not a global bias; the bias in the MACC AOD_{550} depends on the region (Benedictow et al., 2014).

Over the UAE, the overall comparison between MACC AOD_{550} and AERONET AOD_{550} is shown in the scatter density plot in Fig. 11. Generally there is a high overestimation in the MACC AOD_{550}, where the relative bias is +27%. The overall coefficient of determination is 0.634 and the relative RMSE is high at 48%. These deviations may lead to significant errors in the McClear estimated irradiances.

Oumbe et al. (2012a) computed the time series of the GHI and the DNI at each AERONET station using the radiative transfer model libRadtran: once with the AERONET computed AOD_{550} and once with the MACC AOD_{550}. The comparison between the resulting irradiances gives an estimate on the errors in McClear irradiances that can be attributed to the MACC AOD_{550}. Using the irradiances computed with the AERONET AOD_{550} as the references, they found that errors are low for the GHI (relative bias of −3% and relative RMSE of 5%), but significantly higher for the DNI (relative bias of −12% and relative RMSE of 20%). They concluded that one main source of the errors in McClear originates from the MACC AOD in agreement with the present article.

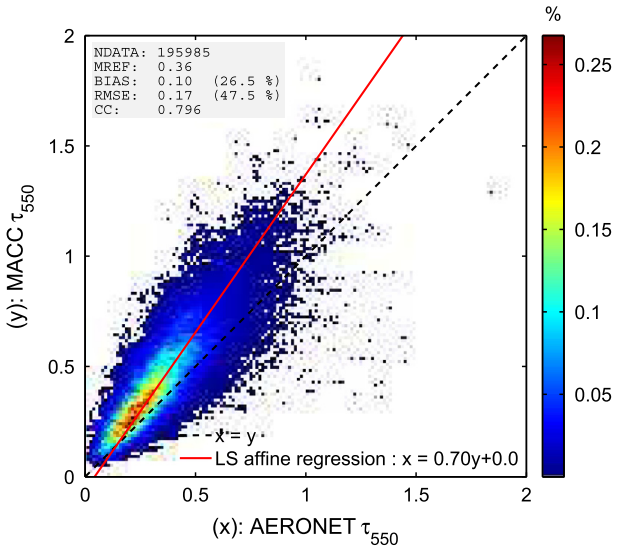

Fig. 11. Scatter density plot between MACC AOD_{550} (τ_{550}) and AERONET AOD_{550} (τ_{550}) for all stations in the UAE.

In the framework of the PREDISOL project, MACC AODs have been identified as the most appropriate aerosol data sets for irradiance estimations in the UAE (Oumbe et al., 2013). They are provided with a relatively high temporal frequency –3 h– and date back to 2004 and will be long-term maintained, as part of an EU-funded project. Compared to the Model of Atmospheric Transport and Chemistry (MATCH, Collins et al., 2001), another high frequency and global AOD data set, the MACC AODs exhibit a relatively lower deviation when compared to AERONET measurements (Schroedter-Homscheidt and Oumbe, 2013). Only MACC and MATCH were tested over the UAE during the time span of PREDISOL, therefore more research is necessary to assess the performance of other chemical transport models over this region.

4.2. Comparisons with other modelled irradiances for cloud-free conditions

McClear is now compared against two models from the literature predicting irradiances under cloud-free skies in order to further evaluate its performance over the UAE. The first one is the clear sky model of the European Solar Radiation Atlas (ESRA), which is used in the Heliosat-2 model (Rigollier et al., 2000). This model is an empirical one, based on a database of climatological monthly means of Linke turbidity. The GHI from the ESRA model is available in the HelioClim-3v4 (HC3v4) database (Blanc

Table 6
Validations of cloud-free global horizontal irradiances by E-ANN, HC3v4 and McClear. Overall is for all measurements from all stations combined.

Station	Model	# of samples	Mean	Bias		RMSE		R^2
			W m^{-2}	W m^{-2}	%	W m^{-2}	%	
AR	E-ANN	5599	631.1	−55	−9	71	11	0.962
	HC3v4	7955	637.9	−31	−5	43	7	0.992
	McClear	7955	637.9	−9	−1	29	5	0.986
EJH	E-ANN	6782	604.6	−8	−1	43	7	0.962
	HC3v4	9090	609.0	−10	−2	27	5	0.990
	McClear	9090	609.0	+9	+1	25	4	0.988
MasdC	E-ANN	5344	544.3	−31	−6	64	12	0.925
	HC3v4	7241	557.6	+6	+1	28	5	0.984
	McClear	7241	557.6	+35	+6	47	8	0.980
MZ_{masd}	E-ANN	2806	549.8	−42	−8	61	11	0.951
	HC3v4	4755	582.1	−4	−1	20	3	0.992
	McClear	4755	582.1	+18	+3	29	5	0.990
MZ_{bertin}	E-ANN	2806	568.2	−60	−11	73	13	0.956
	HC3v4	4755	603.3	−26	−4	36	6	0.992
	McClear	4755	603.3	−5	−1	22	4	0.990
SW	E-ANN	6106	577.2	−29	−5	55	10	0.951
	HC3v4	8230	585.1	−13	−2	29	5	0.990
	McClear	8230	585.1	+18	+3	31	5	0.988
WA	E-ANN	6750	608.5	−51	−8	70	11	0.955
	HC3v4	9320	618.3	−17	−3	31	5	0.992
	McClear	9320	618.3	−1	0	25	4	0.988
Overall	E-ANN	36193	588.9	−37	−6	62	11	0.947
	HC3v4	51346	601.1	−14	−2	32	5	0.988
	McClear	51346	601.1	+9	+2	31	5	0.982

Table 7
Validations of cloud-free direct normal irradiances by E-ANN, HC3v4 and McClear. Overall is for all measurements from all stations combined.

Station	Model	# of samples	Mean	Bias		RMSE		R^2
			W m^{-2}	W m^{-2}	%	W m^{-2}	%	
AR	E-ANN	5599	682.0	−93	−14	138	20	0.667
	HC3v4	7955	689.9	−4	−1	87	13	0.771
	McClear	7955	689.9	−57	−8	87	13	0.846
EJH	E-ANN	6782	681.3	−19	−3	103	15	0.672
	HC3v4	9090	682.8	+14	+2	81	12	0.736
	McClear	9090	682.8	−15	−2	62	9	0.850
MasdC	E-ANN	5344	628.8	−32	−5	141	23	0.402
	HC3v4	7241	634.2	+23	+4	85	14	0.656
	McClear	7241	634.2	+6	+1	62	10	0.830
MZ_{masd}	E-ANN	2806	659.3	−83	−13	127	19	0.728
	HC3v4	4755	670.3	+15	+2	77	12	0.794
	McClear	4755	670.3	−25	−4	64	10	0.863
MZ_{bertin}	E-ANN	2806	670.5	−94	−14	136	20	0.724
	HC3v4	4755	680.9	+3	0	80	12	0.783
	McClear	4755	680.9	−42	−6	74	11	0.857
SW	E-ANN	6106	657.0	−40	−6	121	18	0.605
	HC3v4	8230	660.1	−2	0	85	13	0.687
	McClear	8230	660.1	−16	−2	63	10	0.850
WA	E-ANN	6750	664.6	−88	−13	141	21	0.645
	HC3v4	9320	668.4	+30	+4	87	13	0.785
	McClear	9320	668.4	−41	−6	74	11	0.861
Overall	E-ANN	36193	663.8	−59	−9	129	19	0.607
	HC3v4	51346	669.5	+12	+2	84	13	0.734
	McClear	51346	669.5	−27	−4	70	11	0.837

et al., 2011). The other model is the ensemble artificial neural network (E-ANN) model, which is a statistical model utilizing the Meteosat Second Generation images for irradiance prediction specifically over the region of the UAE (Eissa et al., 2013). The E-ANN model does not require any aerosol information, but it does require a training beforehand. In this case it was trained using the same training set used by Eissa et al. made of observations in three stations for the year 2010 in the UAE. These two models have been selected because on the one hand, HelioClim-3 is available as a service like McClear and is widely used and known, and on the other hand, the E-ANN model has been specifically developed for the UAE and should offer high performances.

The validation results of those two models are presented for the year 2012 for the seven stations. Ideally there should be an equal number of samples at each of the seven stations. However, the number of validation samples from the E-ANN model is less than those of McClear and HC3v4. There were some gaps in the downloaded Meteosat images, with the most significant being from 12/09/2012 to 27/10/2012. A fair comparison between McClear and HC3v4, and an indication on where the E-ANN model stands with respect to the other two models, is provided herein.

The validation results of the GHI and DNI for the seven stations are respectively presented in Tables 6 and 7. McClear exhibits better statistical indicators in GHI for

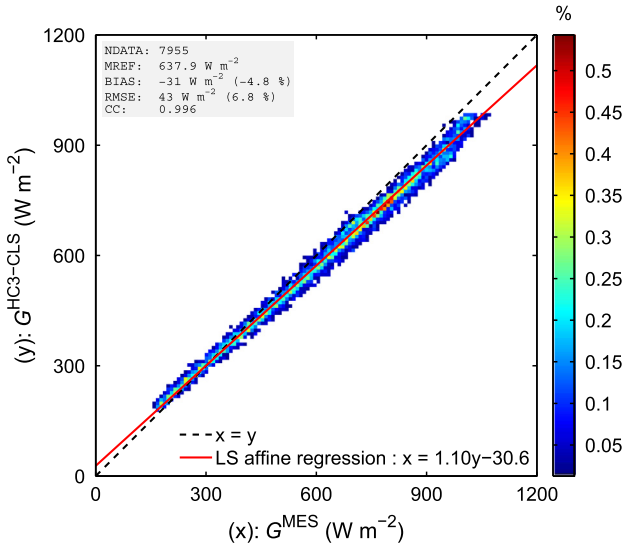

Fig. 12. Scatter density plot of HelioClim-3v4 ($G^{HC3\text{-}CLS}$) versus RSI (G^{MES}) global horizontal irradiance over Al Aradh, 2012.

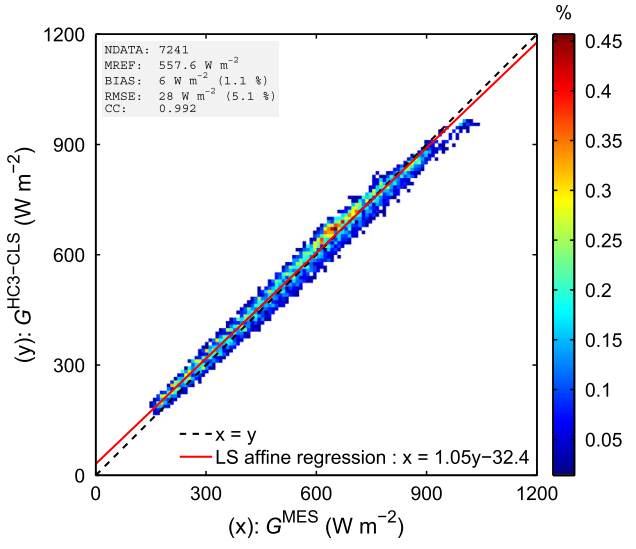

Fig. 13. Scatter density plot of HelioClim-3v4 ($G^{HC3\text{-}CLS}$) versus RSI (G^{MES}) global horizontal irradiance over Masdar City, 2012.

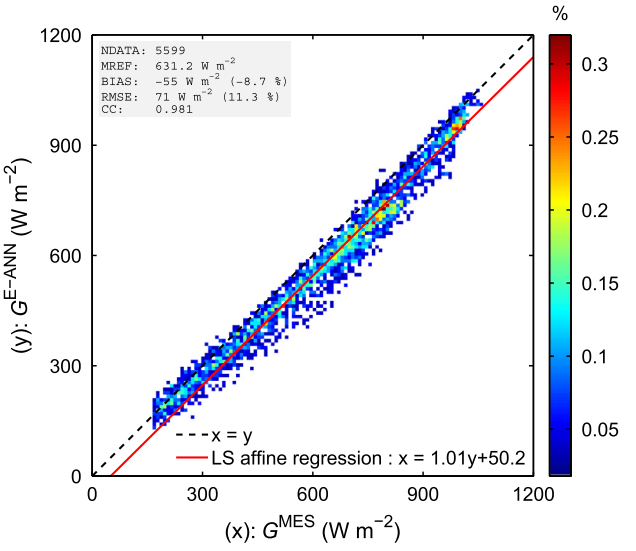

Fig. 14. Scatter density plot of E-ANN ($G^{E\text{-}ANN}$) versus RSI (G^{MES}) global horizontal irradiance over Al Aradh, 2012.

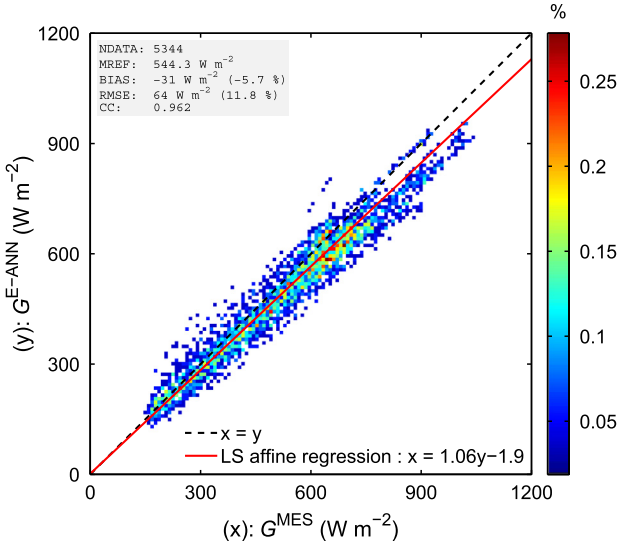

Fig. 15. Scatter density plot of E-ANN ($G^{E\text{-}ANN}$) versus RSI (G^{MES}) global horizontal irradiance over Masdar City, 2012.

AR, EJH, MZ_{bertin} and WA stations, while HC3v4 performs better for MasdC, MZ_{masd} and SW stations. The E-ANN model exhibits the lowest performance. In addition to Figs. 2 and 6, the scatter density plots of the GHI are shown in Fig. 12 (HC3v4 AR), Fig. 13 (HC3v4 MasdC), Fig. 14 (E-ANN AR) and Fig. 15 (E-ANN MasdC). The scatter around the 1:1 line is small in all figures with a negative bias present over AR for all three models. For MasdC, the relative bias for HC3v4 is low (+1%), while it is more significant for the E-ANN model (−6%) and McClear (+6%). The errors of the three models are reasonable, given the uncertainty of the RSI instrument.

For the validations of the DNI, performance of McClear is always better in terms of R^2 and relative RMSE. HC3v4 exhibits the best relative bias for five stations (AR, MZ_{bertin}, MZ_{masd}, SW and WA). The scatter density plots are shown in Fig. 16 (HC3v4 AR), Fig. 17 (HC3v4 MasdC), Fig. 18 (E-ANN AR) and Fig. 19 (E-ANN MasdC).

Even though the GHI estimates from McClear and HC3v4 exhibit similar results –for all stations combined: relative RMSE of 5% for both models, relative bias of −2% and + 2% respectively for HC3v4 and McClear, R^2 of 0.988 and 0.982,- the differences are more pronounced in the DNI –for all stations combined: relative RMSE of 13% and 11% respectively, relative bias of +2% and −4%, R^2 of 0.734 and 0.837. –The higher scatter of samples around the 1:1 line shown in Figs. 16 and 17, as opposed to

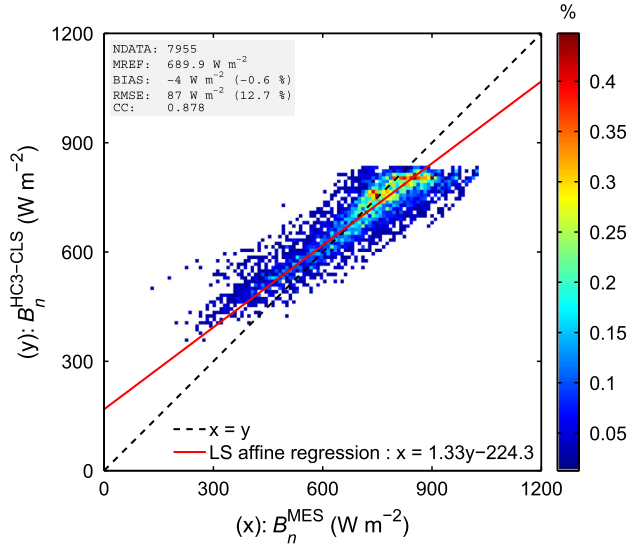

Fig. 16. Scatter density plot of HelioClim-3v4 ($B_n^{HC3-CLS}$) versus RSI (B_n^{MES}) direct normal irradiance over Al Aradh, 2012.

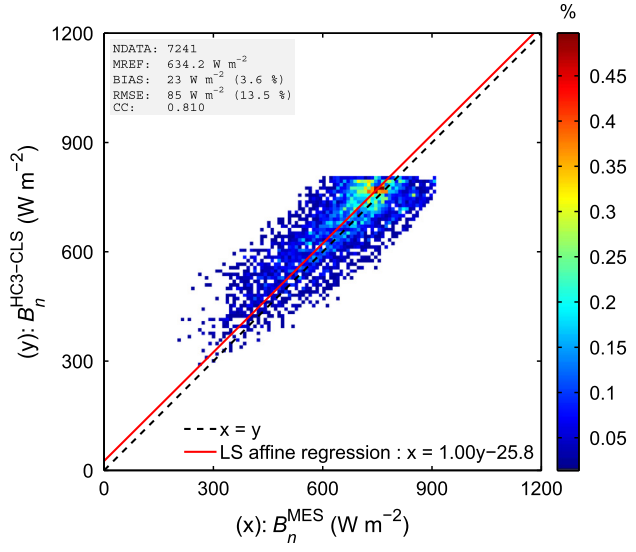

Fig. 17. Scatter density plot of HelioClim-3v4 ($B_n^{HC3-CLS}$) versus RSI (B_n^{MES}) direct normal irradiance over Masdar City, 2012.

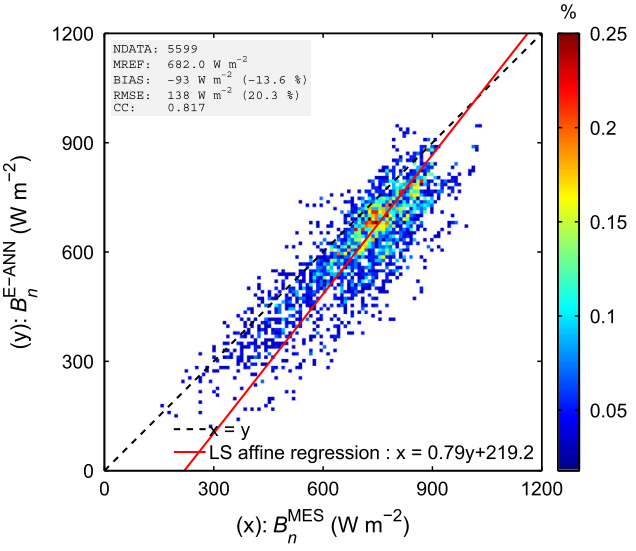

Fig. 18. Scatter density plot of E-ANN (B_n^{E-ANN}) versus RSI (B_n^{MES}) direct normal irradiance over Al Aradh, 2012.

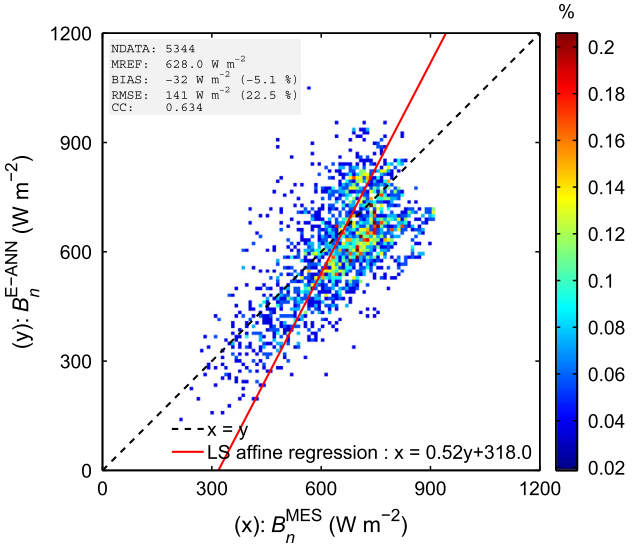

Fig. 19. Scatter density plot of E-ANN (B_n^{E-ANN}) versus RSI (B_n^{MES}) direct normal irradiance over Masdar City, 2012.

those shown in Figs. 3 and 7, can be attributed to the climatological monthly means of the Linke turbidity used in the ESRA model. This suggests that the temporal variation of the McClear DNI is well-reproduced by the 3 hourly time series of the AOD from MACC.

5. Conclusion

This first validation of the McClear model for the specific climate of the United Arab Emirates, where skies are frequently cloud-free but turbid, reveals very satisfactory results as a fast look-up-table-based implementation of a radiative transfer model for the direct and global irradiances. The comparisons between the McClear estimates and measurements of global horizontal and direct normal irradiances for 7 stations show that a large correlation is attained. For 10 min averages of the global horizontal irradiance, the coefficient of determination ranges from 0.980 to 0.990. The bias comprises between $-9\ W\ m^{-2}$ (-1%) and $+35\ W\ m^{-2}$ ($+6\%$), and the RMSE between $22\ W\ m^{-2}$ (4%) to $47\ W\ m^{-2}$ (8%). For the direct normal irradiance, the coefficient of determination ranges from 0.830 to 0.863. The bias comprises between $-57\ W\ m^{-2}$ (-8%) and $+6\ W\ m^{-2}$ ($+1\%$), and the RMSE between $62\ W\ m^{-2}$ (9%) to $87\ W\ m^{-2}$ (13%). The large coefficient of determination and the low standard deviation, computed from the RMSE and bias, demonstrate that McClear offers accurate estimates of the changes of the surface solar irradiance in time.

Comparisons with other models from the literature show that McClear offers similar or better performances. Nevertheless, performances are still far from WMO standards: bias less than $3\ W\ m^{-2}$ and 95% of the deviations less than $20\ W\ m^{-2}$ (WMO, 2010). There is still room for improving the McClear irradiance estimates, mainly for the direct irradiance component which is underestimated for six of the seven stations. This could be done by improving, at least locally, the MACC-derived aerosol properties and adding more information on the circumsolar radiation.

Work is in progress to estimate the circumsolar radiation in an efficient manner for given atmospheric conditions (Blanc et al., 2014a; Eissa et al., 2014). Incorporating knowledge on the circumsolar radiation in McClear would improve the quality of the assessments, particularly for the concentrating solar technologies, i.e. concentrated photovoltaic and concentrated solar thermal electric systems.

Acknowledgments

This work partly took place within the PREDISOL project funded by Total New Energies. The research leading to these results has partly received funding from the European Union's Seventh Framework Programme (FP7/2007-2013) under grant agreement no. 218793 (MACC project) and no. 283576 (MACC-II project). The authors thank the team developing the radiative transfer model libRadtran (http://www.libradtran.org). The authors also thank Masdar Clean Energy and Bertin Technologies for the solar radiation measurements across the UAE and all the personnel who installed and maintained the AERONET stations in the UAE. The authors also thank the anonymous reviewers for their valuable comments which improved the quality of this work.

References

Al Jaber, S.A., 2013. MENA energy transition strategy: a call for leadership in energy innovation. Energy Strategy Reviews 2, 5–7, <http://dx.doi.org/10.1016/j.esr.2012.11.009>.

Anderson, G.P., Clough, S.A., Kneizys, F.X., Chetwynd, J.H., Shettle, E.P., 1986. AFGL atmospheric constituent profiles (0-120km). Tech. Rep. AFGL-TR-86-0110, Air Force Geophys. Lab., Hanscom Air Force Base, Bedford, Mass., USA. <http://www.dtic.mil/cgi-bin/GetTRDoc?AD=ADA175173> (last access: 6 March 2014).

Ångström, A., 1964. The parameters of atmospheric turbidity. Tellus 16, 64–75, <http://dx.doi.org/10.1111/j.2153-3490.1964.tb00144.x>.

Benedetti, A., Morcrette, J.-J., Boucher, O., Dethof, A., Engelen, R.J., Fisher, M., Flentje, H., Huneeus, N., Jones, L., Kaiser, J.W., Kinne, S., Mangold, A., Razinger, M., Simmons, A.J., Suttie, M., 2009. Aerosol analysis and forecast in the European Centre for Medium-Range Weather Forecasts Integrated Forecast System: 2. Data assimilation. J. Geophys. Res. 114, D13205, <http://dx.doi.org/10.1029/2008JD011115>.

Benedictow, A., Blechschmidt, A.M., Bouarar, I., Botek, E., Chabrillat, S., Christophe, Y., Cuevas, E., Clark, H., Flentje, H., Gaudel, A., Griesfeller, J., Huijnen, V., Huneeus, N., Jones, L., Kapsomenakis, J., Kinne, S., Langerock, B., Lefever, K., Razinger, M., Richter, A., Schulz, M., Thomas, W., Thouret, V., Vrekoussis, M., Wagner, A., Zerefos, C., 2014. Validation report of the MACC reanalysis of global atmospheric composition: Period 2003-2012. Tech. Rep., MACC-II Project. <https://www.gmes-atmosphere.eu/documents/maccii/deliverables/val/MACCII_VAL_DEL_D_83.6_REAreport04_20140729.pdf> (last access: 11 September 2014).

Blanc, P., Wald, L., 2012. The SG2 algorithm for a fast and accurate computation of the position of the Sun for multi-decadal time period. Sol. Energy 86, 3072–3083, <http://dx.doi.org/10.1016/j.solener.2012.07.018>.

Blanc, P., Gschwind, B., Lefevre, M., Wald, L., 2011. The HelioClim Project: surface solar irradiance data for climate applications. Remote Sensing 3, 343–361, <http://dx.doi.org/10.3390/rs3020343>.

Blanc, P., Espinar, B., Geuder, N., Gueymard, C., Meyer, R., Pitz-Paal, R., Reinhardt, B., Renne, D., Sengupta, M., Wald, L., Wilbert, S., 2014a. Direct normal irradiance related definitions and applications: the circumsolar issue. Sol. Energy 110, 561–577, <http://dx.doi.org/10.1016/j.solener.2014.10.001>.

Blanc, P., Gschwind, B., Lefevre, M., Wald, L., 2014b. Twelve monthly maps of ground albedo parameters derived from MODIS data sets. In: Proceedings of IGARSS 2014, held 13–18 July 2014, Quebec, Canada, USBKey, pp. 3270–3272. <http://dx.doi.org/10.1109/IGARSS.2014.6947177>.

Buie, D., Monger, A.G., Dey, C.J., 2003. Sunshape distributions for terrestrial solar simulations. Sol. Energy 74, 113–122, <http://dx.doi.org/10.1016/S0038-092X(03)00125-7>.

Cano, D., Monget, J., Albuisson, M., Guillard, H., Regas, N., Wald, L., 1986. A method for the determination of the global solar radiation from meteorological satellite data. Sol. Energy 37, 31–39, <http://dx.doi.org/10.1016/0038-092X(86)90104-0>.

Collins, W.D., Rasch, P.J., Eaton, B.E., Khattatov, B.V., Lamarque, J.-F., Zender, C.S., 2001. Simulating aerosols using a chemical transport model with assimilation of satellite aerosol retrievals: methodology for INDOEX. J. Geophys. Res. 106, 7313–7336, <http://dx.doi.org/10.1029/2000JD900507>.

Eissa, Y., Chiesa, M., Ghedira, H., 2012. Assessment and recalibration of the Heliosat-2 method in global horizontal irradiance modeling over the desert environment of the UAE. Sol. Energy 86, 1816–1825, <http://dx.doi.org/10.1016/j.solener.2012.03.005>.

Eissa, Y., Marpu, P.R., Gherboudj, I., Ghedira, H., Ouarda, T.B.M.J., Chiesa, M., 2013. Artificial neural network based model for retrieval of the direct normal, diffuse horizontal and global horizontal irradiances using SEVIRI images. Sol. Energy 89, 1–16, <http://dx.doi.org/10.1016/j.solener.2012.12.008>.

Eissa, Y., Blanc, P., Oumbe, A., Ghedira, H., Wald, L., 2014. Estimation of the circumsolar ratio in a turbid atmosphere. 2013 ISES Solar World Congress, 3-7 November 2013, Cancun, Mexico. Energy Procedia, 57, 1169–1178. <http://dx.doi.org/10.1016/j.egypro.2014.10.104>.

Geuder, N., Affolter, R., Kraas, B., Wilbert, S., 2014. Long-term behavior, accuracy and drift of LI-200 pyranometers as radiation sensors in Rotating Shadowband Irradiometers (RSI). Proceedings of SolarPACES Conference, 17–20 September 2013, Las Vegas, USA. Energy Procedia 49, 2330–2339. http://dx.doi.org/10.1016/j.egypro.2014.03.247>.

Gherboudj, I., Ghedira, H., 2014. Spatiotemporal assessment of dust loading over the United Arab Emirates. Int. J. Climatol., <http://dxdoi.org/10.1002/joc.3909>.

Gueymard, C.A., 2012. Clear-sky irradiance predictions for solar resource mapping and large-scale applications: Improved validation methodology and detailed performance analysis of 18 broadband radiative models. Sol. Energy 86, 2145–2169, <http://dx.doi.org/10.1016/j.solener.2011.11.011>.

Hess, M., Koepke, P., Schult, I., 1998. Optical properties of aerosols and clouds: the software package OPAC. Bull. Am. Meteorol. Soc. 79, 831–844, <http://dx.doi.org/10.1175/1520-0477(1998)079<0831:OPOAAC>2.0.CO;2>.

Holben, B.N., Eck, T.F., Slutsker, I., Tanre, D., Buis, J.P., Setzer, A., Vermote, E., Reagan, J.A., Kaufman, Y.J., Nakajima, T., Lavenu, F., Jankowiak, I., Smirnov, A., 1998. AERONET — a federated instrument network and data archive for aerosol characterization. Remote Sens. Environ. 66, 1–16, <http://dx.doi.org/10.1016/S0034-4257(98)00031-5>.

Ineichen, P., 2006. Comparison of eight clear sky broadband models against 16 independent data banks. Sol. Energy 80, 468–478, <http://dx.doi.org/10.1016/j.solener.2005.04.018>.

Inness, A., Baier, F., Benedetti, A., Bouarar, I., Chabrillat, S., Clark, H., Clerbaux, C., Coheur, P., Engelen, R.J., Errera, Q., Flemming, J., George, M., Granier, C., Hadji-Lazaro, J., Huijnen, V., Hurtmans, D., Jones, L., Kaiser, J.W., Kapsomenakis, J., Lefever, K., Leitão, J., Razinger, M., Richter, A., Schultz, M.G., Simmons, a.J., Suttie, M., Stein, O., Thépaut, J.-N., Thouret, V., Vrekoussis, M., Zerefos, C., 2013. The MACC reanalysis: an 8 yr data set of atmospheric composition. Atmos. Chem. Phys. 13, 4073–4109, <http://dx.doi.org/10.5194/acp-13-4073-2013>.

Lefevre, M., Oumbe, A., Blanc, P., Espinar, B., Gschwind, B., Qu, Z., Wald, L., Schroedter-Homscheidt, M., Hoyer-Klick, C., Arola, A., Benedetti, A., Kaiser, J.W., Morcrette, J.-J., 2013. McClear: a new model estimating downwelling solar radiation at ground level in clear-sky conditions. Atmos. Measur. Tech. 6, 2403–2418, <http://dx.doi.org/10.5194/amt-6-2403-2013>.

Long, C.N., Ackerman, T.P., 2000. Identification of clear skies from broadband pyranometer measurements and calculation of downwelling shortwave cloud effects. J. Geophys. Res. 105, 15609–15626, <http://dx.doi.org/10.1029/2000JD900077>.

Mayer, B., Kylling, A., 2005. Technical note: The libRadtran software package for radiative transfer calculations - description and examples of use. Atmos. Chem. Phys. 5, 1855–1877, <http://dx.doi.org/10.5194/acp-5-1855-2005>.

Mayer, B., Kylling, A., Emde, C., Hamann, U., Buras, R., 2012. libRadtran user's guide. <http://www.libradtran.org/doc/libRadtran.pdf> (last access: 6 March 2014).

Mezher, T., Goldsmith, D., Choucri, N., 2011. Renewable energy in Abu Dhabi: opportunities and challenges. J. Energy Eng. 137, 169–176, <http://dx.doi.org/10.1061/(ASCE)EY.1943-7897.0000042>.

Mokri, A., Aal Ali, M., Emziane, M., 2013. Solar energy in the United Arab Emirates: a review. Renew. Sustain. Energy Rev. 28, 340–375, <http://dx.doi.org/10.1016/j.rser.2013.07.038>.

Ohmura, A., Dutton, E.G., Forgan, B., Fröhlich, C., Gilgen, H., Hegner, H., Heimo, A., König-Langlo, G., McArthur, B., Müller, G., Philipona, R., Pinker, R., Whitlock, C.H., Dehne, K., Wild, M., 1998. Baseline Surface Radiation Network (BSRN/WCRP): New precision radiometry for climate research. Bull. Am. Meteorol. Soc. 79, 2115–2136, http://dx.doi.org/10.1175/1520-0477(1998)079<2115:BSRNBW>2.0.CO;2.

Oumbe, A., Bru, H., Hassar, Z., Blanc, P., Wald, L., Fournier, A., Goffe, D., Chiesa, M., Ghedira, H., 2012a. Selection and implementation of aerosol data for the prediction of solar resource in United Arab Emirates. Proceedings of SolarPACES Conference, 11–14 September 2012, Marrakech, Morocco. PSE AG, Freiburg, Germany, USBKey, Paper#22240. <http://hal-ensmp.archives-ouvertes.fr/docs/00/77/97/49/PDF/2012_oumbe_aerosol_uae_solarpaces.pdf> (last access: 10 September 2014).

Oumbe, A., Qu, Z., Blanc, P., Bru, H., Lefevre, M., Wald, L., 2012b. Modeling circumsolar irradiance to adjust beam irradiances from radiative transfer models to measurements. EMS Annual Meeting, 10–12 September 2012, Lodz, Poland. <http://www.endorse-fp7.eu/sites/www.endorse-fp7.eu/files/docs/Poster_EMS2012_CRS_V2.2.pdf> (last access: 6 March 2014).

Oumbe, A., Bru, H., Hassar, Z., Blanc, P., Wald, L., Eissa, Y., Marpu, P., Gherboudj, I., Ghedira, H., Goffe, D., 2013. On the improvement of MACC aerosol spatial resolution for irradiance estimation in the United Arab Emirates. 2013 ISES Solar World Congress, 3–7 November 2013, Cancun, Mexico.

Oumbe, A., Qu, Z., Blanc, P., Lefevre, M., Wald, L., Cros, S., 2014. Technical Note - Decoupling the effects of clear atmosphere and clouds to simplify calculations of the broadband solar irradiance at ground level. Geoscientific Model Dev. 7, 1661–1669, <http://dx.doi.org/10.5194/gmd-7-1661-2014>.

Perez, R., Ineichen, P., Moore, K., Kmiecik, M., Chain, C., George, R., Vignola, F., 2002. A new operational model for satellite-derived irradiances: description and validation. Sol. Energy 73, 307–317, <http://dx.doi.org/10.1016/S0038-092X(02)00122-6>.

Qu, Z., Blanc, P., Lefevre, M., Wald, L., Watts, P., Schroedter-Homscheidt, M., Gesell, G., Klueser, L., 2012a. Use of OCA and APOLLO in Heliosat-4 method for the assessment of surface downwelling solar irradiance. Proceedings of the 2012 EUMETSAT Meteorological Satellite Conference, EUMETSAT P.61, paper S2-03, 3–7 September 2012, Sopot, Poland. <https://www.eumetsat.int/website/wcm/idc/idcplg?IdcService=GET_FILE&dDocName=PDF_CONF_P61_S2_03_QU_V&RevisionSelectionMethod=LatestReleased&Rendition=Web> (last access: 6 March 2014).

Qu, Z., Oumbe, A., Blanc, P., Lefevre, M., Wald, L., Schroedter-Homscheidt, M., Gesell, G., Klueser, L., 2012b. Assessment of Heliosat-4 surface solar irradiance derived on the basis of SEVIRI-APOLLO cloud products. Proceedings of the 2012 EUMETSAT Meteorological Satellite Conference, EUMETSAT P.61, paper S2-06, 3–7 September 2012, Sopot, Poland. <http://www.eumetsat.int/website/wcm/idc/idcplg?IdcService=GET_FILE&dDocName=PDF_CONF_P61_S2_06_QU_P&RevisionSelectionMethod=LatestReleased&Rendition=Web> (last access: 6 March 2014).

Reid, J., Piketh, S., Kahn, R., Bruintjes, R., Holben, B., 2005. A summary of first year activities of the United Arab Emirates Unified Aerosol Experiment: UAE^2. Tech. Rep., NRL/MR/7534–05-8899. <http://uae2.gsfc.nasa.gov/MR8899UAE2.pdf> (last access: 6 March 2014).

Rigollier, C., Bauer, O., Wald, L., 2000. On the clear sky model of the ESRA — European Solar Radiation Atlas — with respect to the Heliosat method. Sol. Energy 68, 33–48, <http://dx.doi.org/10.1016/S0038-092X(99)00055-9>.

Rigollier, C., Lefevre, M., Wald, L., 2004. The method Heliosat-2 for deriving shortwave solar radiation from satellite images. Sol. Energy 77, 159–169, <http://dx.doi.org/10.1016/j.solener.2004.04.017>.

Roesch, A., Wild, M., Ohmura, A., Dutton, E.G., Long, C.N., Zhang, T., 2011. Assessment of BSRN radiation records for the computation of monthly means. Atmos. Measur. Tech. 4, 339–354, <http://dx.doi.org/10.5194/amt-4-339-2011>.

Schaaf, C.B., Gao, F., Strahler, A.H., Lucht, W., Li, X., Tsang, T., Strugnell, N.C., Zhang, X., Jin, Y., Muller, J.-P., Lewis, P., Barnsley, M., Hobson, P., Disney, M., Roberts, G., Dunderdale, M., Doll, C., D'Entremont, R.P., Hu, B., Liang, S., Privette, J.L., Roy, D., 2002. First operational BRDF, albedo nadir reflectance products from MODIS. Remote Sens. Environ. 83, 135–148, <http://dx.doi.org/10.1016/S0034-4257(02)00091-3>.

Schillings, C., Mannstein, H., Meyer, R., 2004. Operational method for deriving high resolution direct normal irradiance from satellite data. Sol. Energy 76, 475–484, <http://dx.doi.org/10.1016/j.solener.2003.07.038>.

Schroedter-Homscheidt, M., Oumbe, A., 2013. Validation of an hourly resolved global aerosol model in answer to solar electricity generation information needs. Atmos. Chem. Phys. 13, 3777–3791, <http://dx.doi.org/10.5194/acp-13-3777-2013>.

Schroedter-Homscheidt, M., Oumbe, A., Benedetti, A., Morcrette, J.-J., 2013. Aerosols for concentrating solar electricity production forecasts: Requirement quantification and ECMWF/MACC aerosol forecast assessment. Bull. Am. Meteorol. Soc. 94, 903–914, <http://dx.doi.org/10.1175/BAMS-D-11-00259.1>.

Sun, Z., Liu, A., 2013. Fast scheme for estimation of instantaneous direct solar irradiance at the Earth's surface. Sol. Energy 98, 125–137, <http://dx.doi.org/10.1016/j.solener.2012.12.013>.

Wilbert, S., Reinhardt, B., DeVore, J.G., Röger, M., Pitz-Paal, R., Gueymard, C.A., Buras, R., 2013. Measurement of solar radiance profiles with the sun and aureole measurement system. J. Sol. Energy Eng. 135, 041002, <http://dx.doi.org/10.1115/1.4024244>.

WMO, 2010. Guide to meteorological instruments and methods of observation. World Meteorological Organization, WMO-No 8 (2010 update), 7th ed., Geneva, Switzerland. <http://library.wmo.int/pmb_ged/wmo_8_en-2012.pdf> (last access: 16 December 2014).

Zelenka, A., Perez, R., Seals, R., Renne, D., 1999. Effective accuracy of satellite-derived hourly irradiances. Theoret. Appl. Climatol. 62, 199–207, <http://dx.doi.org/10.1007/s007040050084>.